VOL. 11, NO. 16, AUGUST 2016 ISSN 1819-6608
ARPN Journal of Engineering and Applied Sciences


www.arpnjournals.com

THE NUMERICAL INVESTIGATION ON THE EFFECTS OF ASPECT RATIO AND CROSS-SECTIONAL SHAPRE ON THE WAKE STRUCTURE BEHIND A CANTILEVER

Hiang Bin Chan[1], Tshun Howe Yong[1], Perumal Kumar[2], Siaw Khur Wee[3] and Sharul Sham Dol[3]
[1]Department of Mechanical Engineering, Curtin University, Malaysia
[2]Department of Chemical Engineering, Curtin University, Malaysia
[3]Department of Petroleum Engineering, Curtin University, Malaysia
E-Mail: sharulsham@curtin.edu.my

ABSTRACT

This paper aims to investigate the effects of aspect ratio (AR) and geometry have on the flow dynamics of a free end finite cylinder via numerical simulation. The AR used in this investigation is AR=3, 5, 7 whilst a circular cantilever cylinder and a rectangular flat plate are used as the geometry. The Reynolds number based on cylinder diameter is 20000. *k-ω* (*SST*) is used to model the turbulence. End tip effects are seen on free end finite cylinder. By studying the velocity defect flux (*Q*), tip effects are found to be independent of AR. They are however limited to 2*D*~3*D* for circular cantilever cylinder and 3*D*~4*D* for rectangular flat plate. Velocity defect is stronger for rectangular flat plate than that of circular cantilever (the range differs from 6.81% to 206.41%) suggesting a stronger vortical activities are present in the wake of rectangular flat plate. It is supported by turbulent kinetic energy (TKE) contours whereby the maximum TKE is approximately 20%~50% higher in rectangular flat plate at each respective AR.

Keywords: cantilever, aspect ratio, cross-sectional shape, wake structure.

INTRODUCTION

Though flow past through a cylinder has been studied as early as in the 1930's, it is still a topic that is of practical interest to many fields of engineering due to the generation of the wake region. The turbulence characteristics in the wake region include higher energy contained vortices, higher magnitude of velocity defect, a shear-layer transition region- all of which, benefit the mixing of fluid. Therefore, the many configurations of the geometry and the wide area of flow dynamics of wake continue to intrigue the interests of many researchers. One of the recent most comprehensive reviews in the last decade was given by Williamson (1996). The development of flow visualization technique unveiled the many different vortical structures in the wake (Dol and Nor, 2006). Besides, the development in computing technology and simulation software helps to get a better understanding of the complex 3-dimensional flow.

The flow dynamics behind a cylinder depends very much on the Reynolds numbers, aspect ratio, and geometry of the cylinder. This is especially true for fixed-free end cylinder, which is also known as a cantilever cylinder. A lot of research (such as Afgan *et al.,* 2007; Afgan *et al.,* 2006; Javadi and Kinai, 2014) has been studied over the past decades as cantilever cylinder has extremely useful application in heat exchangers, offshore platforms, underwater pipelines, gas tanks and etc. A third dominant vortex called the tip vortex develops at the free end of the cantilever cylinder. This poses a complex three-dimensional flow field. Unlike the flow field in the near-wake region of a cylinder, the presence of tip vortex interacts with the Karman and horseshoe vortices that form at the cylinder-wall junction (Afgan *et al.,* 2007)

Afgan *et al.* (2007) simulated the flow physics of the cantilever cylinder of aspect ratio 6 and 10 using Large Eddy Simulation (LES) model. They found different effects for high and low aspect ratios. The effects of the downwash of the two counter rotating vortices near the free end of the cylinder were weaker in high *AR* because the downwash was limited to the top half of the cylinder, hence the interaction was weaker causing the wake behavior to resemble those in the typical two-dimensional flow. This is consistent with the results from Heseltine (2003). In addition to that, Okamoto and Yagita (1973) investigated a cantilever cylinder at $Re=1.3\times10^4$ in wind tunnel. They found that the range of effect of the free end was limited to three diameters from the top of the cylinder.

Ringuette, Mikano and Gharib (2007) studied the vortex formation of rectangular flat plate of aspect ratio of 2 and 6. The flat plate was towed in the water and the flow velocity was captured using digital particle image velocimetry. They found that the vortical structures behind the rectangular flat plate behaved in the total opposite direction than that of the cantilever circular cylinder. They noticed that the effects of tip became more significant and the tip evolved more quickly at lower AR.

Complex three-dimensional wakes are less studied by researchers compared to two-dimensional problems. There are only several others who investigated complex three-dimensional flow experimentally and numerically (Afgan *et al*., 2007; Roh and Park, 2003; Krajnović, 2011; Palau-Salvador *et al.,* 2010) at Re~ $\times10^4$. Though their works have undoubtedly showed insight to the flow dynamics of complex three-dimensional flow, more researches are needed to support the fact that the tip effects has a spanwise limit at is independent to *AR*. Therefore, there is a need to find out the governing parameters that affect the effective region of the tip vortex in a more detail manner. In this regard,

this work aims to use CFD numerical simulations to deepen the understanding on the flow dynamics influenced by different aspect ratio and geometry of the rigid cantilever through studying the velocity profile and relate it to the turbulent kinetic budget equation. Star-CCM+ is used to perform the simulations that are presented in this paper.

This work also serves as a preliminary study to understand complex fluid dynamics of the flexible cantilever (a Fluid-Structure-Interaction) in future investigation.

NUMERICAL MODEL SETUP

Problem definition and computational domain

The present work simulates flow past a cantilever cylinder. The Reynolds-averaged-Navier-Stokes (RANS) equation is used to predict the flow structure around a circular cantilever cylinder and a rectangular cantilever flat plate. Three different aspect ratio (*H/D*), AR=3, 5, 7 are investigated. Investigations are done on a cantilever circular cylinder with a diameter of D = 0.02 m, a cantilever rectangular flat plate with a width of W=0.02 m, and the free stream inlet velocity U= 0.89 m/s, giving a diameter based Reynolds number (Re= $\rho UD/\mu$) of approximately 2×10^4. A schematic diagram of the geometry and computational domain is seen in Figure-1. The inlet turbulent intensity, Ti=0.036% is calculated using $0.16\times Re^{-1/8}$.

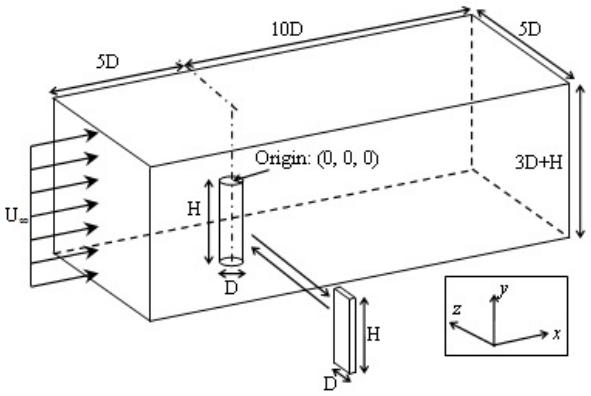

Figure-1. Schematic of the computational domain.

Numerical model

The governing equations are conservation of mass equation, equation (1) and momentum for unsteady incompressible three-dimensional flow. The RANS equation used in Star-CCM+ is shown in equation (2).

$$\frac{\partial \overline{u_i}}{\partial x_i} = 0 \quad (1)$$

$$\rho\left[\frac{\partial \overline{u_i}}{\partial t} + \overline{u_j}\frac{\partial \overline{u_i}}{\partial x_j}\right] = -\frac{\partial \overline{p}}{\partial x_i} + \rho g_i + \frac{\partial}{\partial x_j}\left[\mu\frac{\partial \overline{u_i}}{\partial x_j} - \overline{\rho u_i' u_j'}\right] \quad (2)$$

k-ω (SST) model is used to model the turbulence phenomena. The k-ω (SST) model, developed by Menter (1994), resolves the turbulent viscosity in order to describe the characteristic of turbulent flow that denotes by the Reynolds stresses in *RANS* equation. Unlike standard k-ω model, the k-ω(SST) model integrates standard k-ε and standard k-ω models by introducing a blending function. The standard k-ω resolves the flow in the near wall region, while standard k-ε is used to resolve free-stream turbulence.

The reason k-ω (SST) is chosen in this work is due to its ability to hold both the benefits of k-ω and k-ε simultaneously, as k-ω is more accurate at free stream turbulence but weak at near wall region while *k-ε* vice versa. Though *DNS* would be a more accurate model to simulate the fluid flow problem because of its ability to resolves the flow from Kolmogorov microscale up to the integral scale, an extremely fine mesh is needed. Therefore, a very high computational requirement (even at low Re) is necessary. Apart from that, the fluid-structure interaction (FSI) and complex flow behavior in the later investigation encourage the use of k-ω (SST) that is better in resolving the adverse pressure gradient and discourage the use of DNS. Furthermore, prior to the selection of the model; DES and k-ω (SST) were used to simulate a flow past a fixed-fixed ends cylinder case. The results of stagnation pressure and drag coefficient are then compared with experimental data. The results will be discussed in the Result and Discussion section as part of the model validation.

Mesh independent study is also done to ensure of the optimal mesh. Polyhedral mesh is used in this work. An AR=7 cylinder with Re=2×10^4 case was used. Different set of mesh studies are summarized in Table 1. The maximum dimensionless wall distant, $y+_{max}$ is monitored and ensured that it is smaller than 5 so that the near wall mesh is fine enough to model the viscous sub-layer correctly.

Table-1. Summary of meshes and its respective information.

Mesh No.	Base Size	No. of Cells	Max. $y+$	Drag Coefficient, C_D
Mesh 1	0.006	136979	3.63	0.821
Mesh 2	0.005	149176	3.58	0.841
Mesh 3	0.004	306901	3.34	0.847
Mesh 4	0.003	543050	3.63	0.852
Mesh 5	0.002	1573239	3.71	0.858

To choose the most suitable mesh, the drag coefficient, pressure profile and velocity profile are monitored. The results of the analysis are compiled and presented in Figure-2. Judging from the drag coefficient (C_D), it achieves a near constant value starting from Mesh 2. Further decrease in mesh size does not bring significant impact to the C_D. On the other hand, the velocity profile at x/D=0.75 downstream from the cylinder reaches a consistent pattern starting from Mesh 4. Lastly, based on

the obtained pressure profile at x/D=0.75 downstream, the profiles reach a near consistent pattern starting at Mesh 4 as well. Therefore, based on the overall analysis, Mesh 4 is selected as the most suitable mesh in this work.

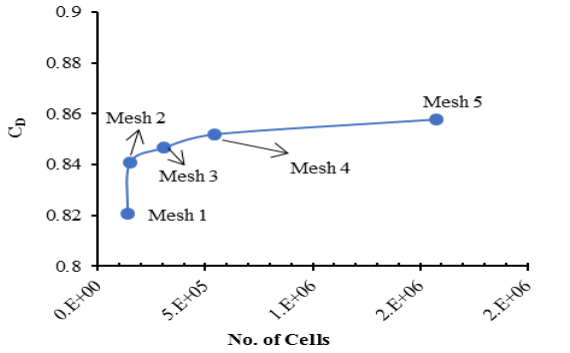

(a)

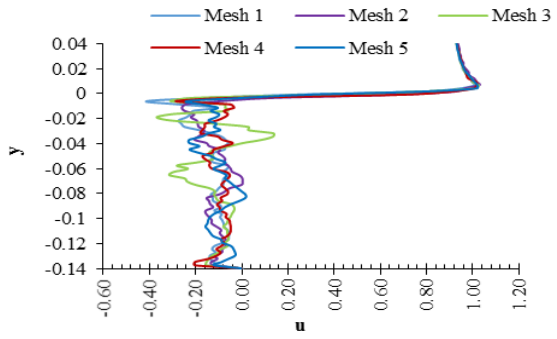

(b)

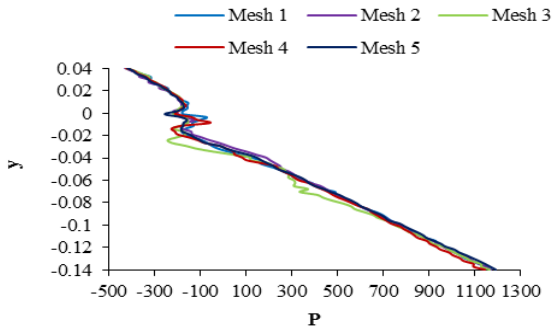

(c)

Figure-2. The mesh independency study: (a) the drag coefficient (C_D); (b) The x-component velocity (u) profile at x/D=0.75 downstream from the cylinder and; (c) The static pressure profile at x/D=0.75 downstream from the cylinder at different mesh conditions.

The size of time step (Δt) is determined from the number of time step ($n_{\Delta t}$) per shedding cycle. The size of time step (Δt) can be calculated by equation (3)

$$\Delta t = \frac{D}{n_{\Delta t}\left(St \times U\right)} \tag{3}$$

where St, D and U represent the Strouhal Number, cylinder's diameter and free stream velocity, respectively. The maximum St possible in this case is 0.21, which is the St for circular cylinder under 2-dimensional flow behavior. For circular cantilever, the St is dependent to the cylinder's length and it is generally lesser than 0.21 due to complex 3-dimensional generated at its free-end. Since the Δt is an inversely proportional to St, the maximum St value (St=0.21) is used in the calculation in order to capture any possible 2-dimensional vortex shedding without compromising the region with slower shedding rate (3-dimensional shedding). It is suggested that at least 20~25 time-steps per shedding cycle are needed to capture vortex shedding correctly. In this work, 53 time-steps per shedding cycle are used so that the shedding can be captured precisely. Thus, by using equation (3), $\Delta t \approx 0.002$s is computed and this value is used in this study.

RESULTS AND DISCUSSIONS

The fluid dynamics become more complex as flow passing over a free end finite cylinder. In order to understand the factors that affect the fluid dynamics of a free end finite cylinder, two different geometries; circular and rectangular shaped cantilever cylinder are used. This paper focuses on the velocity defect of the flow behind a free end finite cylinder to understand the fluid dynamics.

Model validation

A Re≈2.5×10^4 flow past a fixed-fixed end cylinder is simulated and the result is compared with the experimental data. The experiment was conducted using TQ Modular Airflow Bench AF10 subsonic wind tunnel. The pressure along the cylinder surface was obtained. Then the drag coefficient C_D is calculated by using $C_D = \int_0^{2\pi} C_p \cos\theta \delta\theta$. The drag coefficients obtained in both experimental and CFD are compared for validation. Furthermore, Detached Eddy Simulation (DES) is also used to simulate the case. The consideration of many turbulence models in this test is to check the validity of the model, which can be helpful in the selection of the final turbulence model. The summary of the study in tabulated in Table-2.

Based on the study, k-ω (SST) achieves the lowest discrepancy compared to DES. The error between experimental and numerical results modeled by k-ω(SST) is less than 2.49% and 0.81% for Mesh 4 and Mesh 5, respectively; while DES achieves a high - 19.31% discrepancy. Moreover, this study also confirms that Mesh 4 is sufficient and capable to simulate the desire problem since the discrepancy obtained is <3% that is within an acceptable range. Mesh 5 is less recommended because it contains 2.89 times more number of cells compared to Mesh 4 that lead to an approximately 1.8 times longer

computational time, although it has achieved a low 0.81% differences.

Table-1. Details of experimental and CFD comparison.

Mesh No.	Base Size	No. of Cells	Max. $y+$	Drag Coefficient, C_D
Mesh 1	0.006	136979	3.63	0.821
Mesh 2	0.005	149176	3.58	0.841
Mesh 3	0.004	306901	3.34	0.847
Mesh 4	0.003	543050	3.63	0.852
Mesh 5	0.002	1573239	3.71	0.858

Besides, to further proof the reliability of the model, the flow field of the simulated *AR*=5 circular cantilever is compared with the visualization image, under the same flow condition (*i.e.* $Re=2\times10^4$), captured by Park and Lee (2000) (see Figure-3). Due to the fact that the instantaneous numerical result is compared with an instantaneous experimental visualization frame, the flow field may not be perfectly similar. However, both flow fields show a high similarity. In addition, some distinct flow features can be distinguished and identified. These features are grouped accordingly with boxes in different shapes, as shown in Figure 3.

Influence of aspect ratio

The velocity profile of AR = 3, 5, 7 of circular and rectangular cantilever are shown in Figure-4 and Figure-5 respectively. It can be seen that the wake region changes dramatically when AR changes.

An inconsistent velocity gradient along the cantilever's span is observed for circular cylinder. A steep velocity gradient is seen at the region near tip but this phenomenon disappears quickly as it departs from near tip region. The authors regard the near tip region as the region taken effective by the tip effects; a region where the tip vortex plays a role. Any region outside of the near tip region is likely to exhibit a dynamically two dimensional flow field and is not of particular interest of the authors. This behavior becomes more distinct starting from *x/D*=2 for all aspect ratio. This phenomenon is believed to be caused by the tip effects. At the free end of the finite cylinder, the tip can cause the generation of second dominant vortex- the tip vortex. The presence of tip vortex can affect and alter the flow field at the near tip region, resulting in a steep velocity gradient. The double dot-dash arrows in Figure-4 and Figure-5 mark the position where the tip effects begin to diminish. The absence of the double dot-dash arrows in Figure-4(i) and 5(i) shows the whole span in the wake is affected by tip vortex. Hence, the whole profile is considered as the near tip region. With reference to the velocity gradient of the velocity profiles in Figure-4 and Figure-5, the tip effects are presence in approximately *y/D*=-2 to-3 for circular cantilever cylinder whereas z/*D*=-3 to -4 for rectangular flat plate. It is worth noting that there is no relationship between the effective area of the near tip region and the AR for circular finite cylinder and rectangular flat plate. The finding for circular cantilever cylinder is also consistent with the results from Okamoto and Yagita (1973).

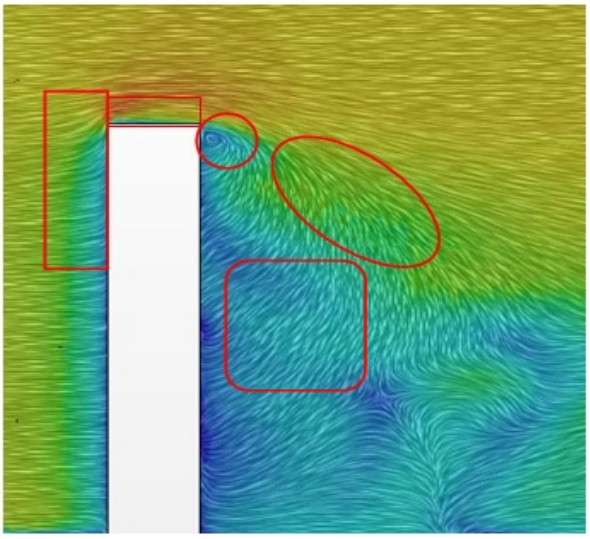

(a)

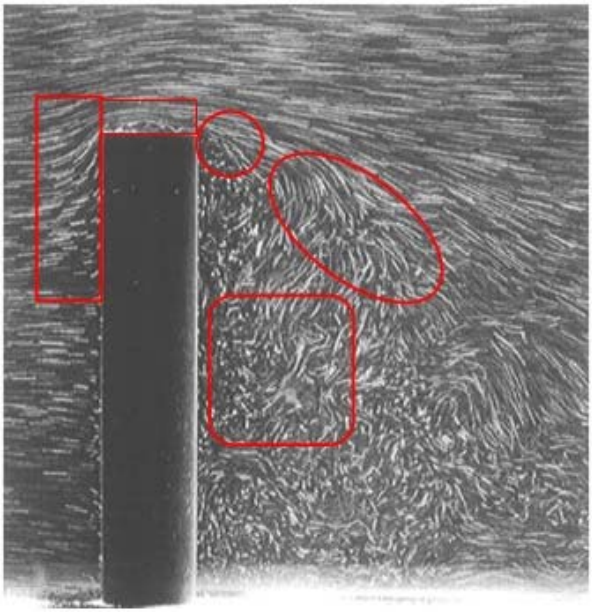

(b)

Figure-3. The instantaneous velocity flow field comparison (at the plane of symmetry) of the *CFD* result with the experimental result: (a) *CFD* (*k-ω* (*SST*) – Mesh 4); (b) experimental visualization (Park and Lee, 2000).

The effects of tip vortex discussed above can also be observed from the vorticity contour (Figure-6 and Figure-7). At lower aspect ratio (*i.e.* AR=3), the flow in the near-wake region exhibits a 'smoother' or less 'bumpy' profile. The vorticity at such location shows less complex-vortical structures, which contributes to a less 'bumpy' velocity profile. According to the contour, it is suspected that most of the vortical structure – von Kármán

vortices are suppressed by the tip vortex in the near tip region. As a result, only tip vortices are observed in the contour for AR=3. As the AR is increasing, von Kármán vortices become more pronounced. Von Kármán vortices can be seen located at the region $y/D < -3$ for AR=5 and 7 for circular cantilever cylinder as opposed to $y/D < -4$ for AR=5 only for rectangular flat plate. The observations are in agreement with the observations made from velocity profile.

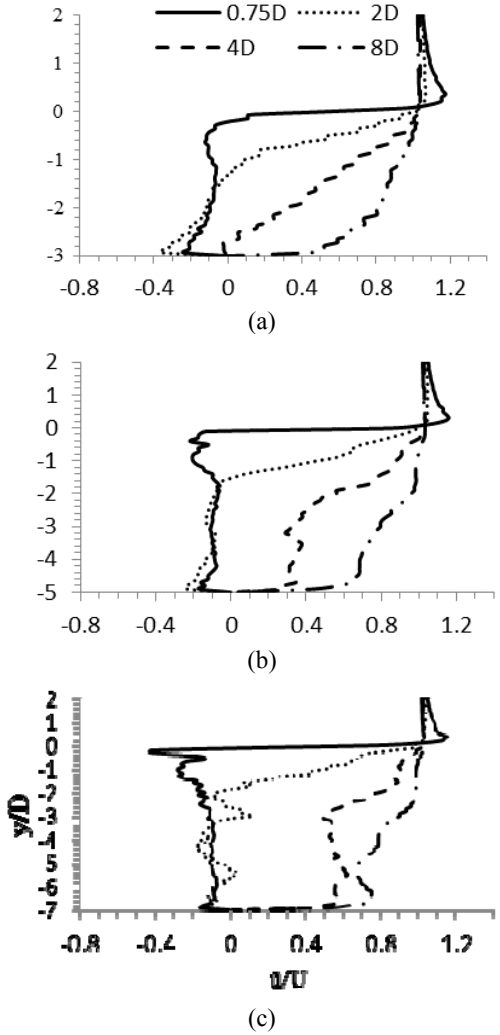

Figure-4. The mean u-velocity (the velocity in x-direction) at the plane of symmetry for circular cantilever, where (i) *AR*=3; (ii) *AR*=5, and (iii) *AR*=7.

Based on Figure-6 and Figure-7, it can be clearly observed that the shedding mode and wake structures are highly dependent on the AR. The wake structure can be divided into two distinct regions: i) the near tip region (region affected by tip vortex; has steep velocity gradient $^{du(y)}/_{dy}$ in the velocity profiles); and ii) the two-dimensional region (region that is free from the effects of the tip vortex; has flat velocity gradient). These regions are distinguished by a dash line in Figure-6 and 7. By comparing both velocity profiles (Figure-4 and 5) and vorticity contours (Figure-6 and 7), it is interesting to notice that the velocity defect is only present in the wake region. Outside of the wake, the velocity of the flow is close to the free stream velocity. In other word, the velocity defect is the product of wake formation. Therefore, it is safe to conclude that the velocity defect is a direct indicator of the presence of the wake or, precisely, the vortical structures in wake.

Besides, the magnitude of the velocity defect is examined to identify the impact of different AR has on the velocity profile. With analogous to velocity flux, commonly known as the volumetric flow rate, the magnitude or the strength of the velocity defect is determined by computing the area-under-the-curves.

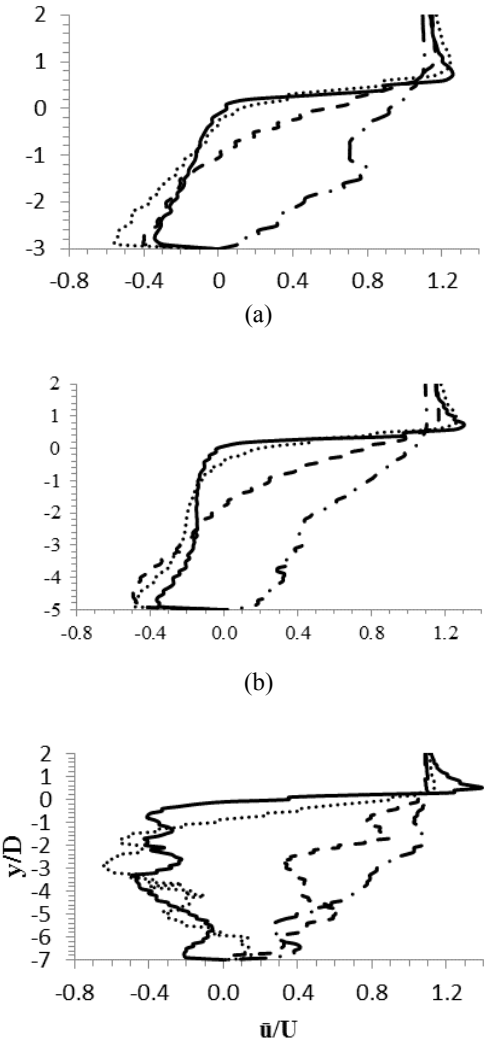

Figure-5. The mean u-velocity (the velocity in x-direction) at the plane of symmetry for Rectangular flat plate, where (a) *AR*=3; (b) *AR*=5, and (c) *AR*=7.

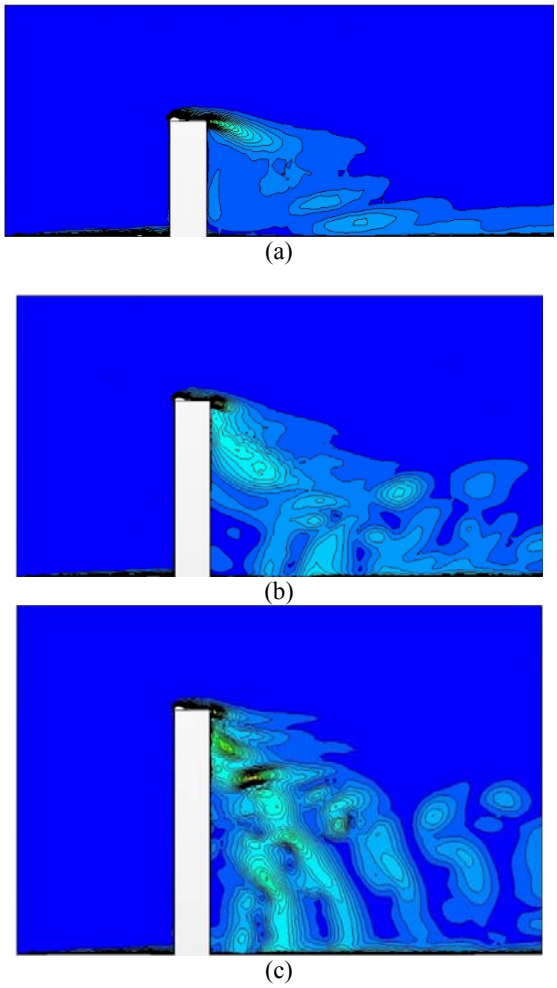

Figure-6. The instantaneous vorticity contour at the plane of symmetry when *t=2s* for circular cantilever, where (a) AR=3; (b) AR=5, and (c) AR=7.

In this case, the area-under-the-curves is the region bounded by the curve of velocity profile and the curve of *U* (represented by the vertical dash lines in Figure 4 and 5).Thus, the magnitude of the velocity defect can also be said as the velocity defect flux. The normalized and dimensionless velocity defect flux, *Q* can be calculated by equation (4):

$$Q = \frac{1}{U}\int_{n}^{0}(U - u(y/D))d\left(y/D\right) \quad (4)$$

where *n*=-3, -5, -7 are the lower limit of the integral for that represent the aspect ratios used in this work. Since this variable describes the defect of velocity with reference to the free stream velocity (*U*), it is a negative term. For the ease of presentation, the absolute value, |*Q*| is used. The results are presented in Figure-8.

Based on Figure-8, it can be seen that the *Q* decreases as it travels downstream indicating the evolution of the velocity in downstream direction. Besides, an increase in velocity defect magnitude is observed when the AR is increased. However, this is due to the increasing span of the cylinder that lead to a more affected region.

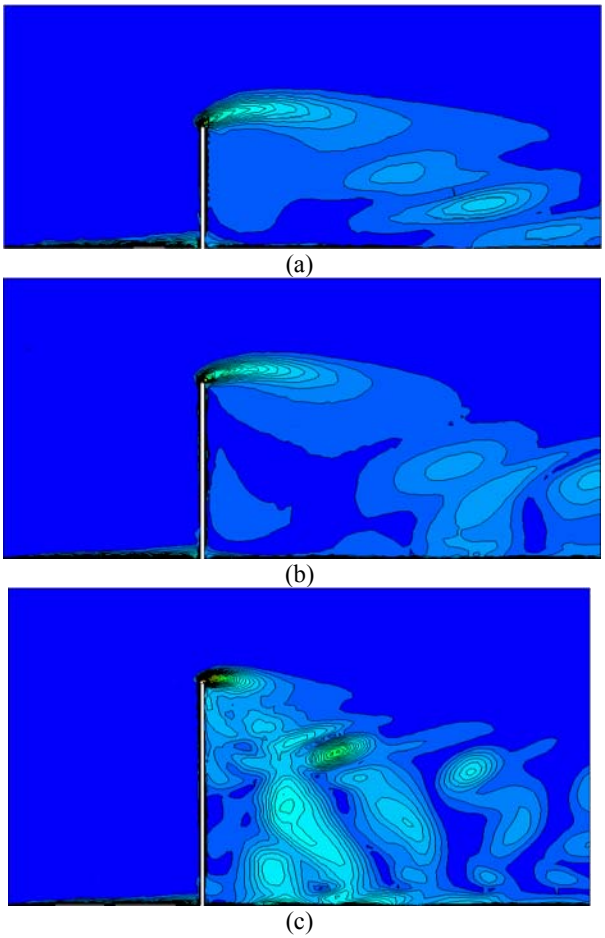

Figure-7. The instantaneous vorticity contour at the plane of symmetry when t=2s for rectangular flat plate, where (a) AR=3; (b) AR=5, and (c) AR=7.

Therefore, in order to accurately examine the contribution of AR, the velocity defect flux is calculated based on the discretized section of the cylinder. In this case, an approximate velocity defect flux at each section is computed by using the trapezoid rule, as shown in equation (5):

$$dQ = \frac{\left(y_n/D - y_{n+1}/D\right)}{2}\left[\left(\frac{u\left(y_n/D\right)}{U} - 1\right) + \left(\frac{u\left(y_{n+1}/D\right)}{U} - 1\right)\right] \quad (4)$$

Where n represents the location along the cylinder's span. The distance between two predetermined locations, $\left(y_n/D - y_{n+1}/D\right)$ is set to be equal to 0.1 in every calculation. The purpose of defining a fix distance in all calculations is to encourage a fair comparison. The computed results are plotted in Figure-9 and 10.

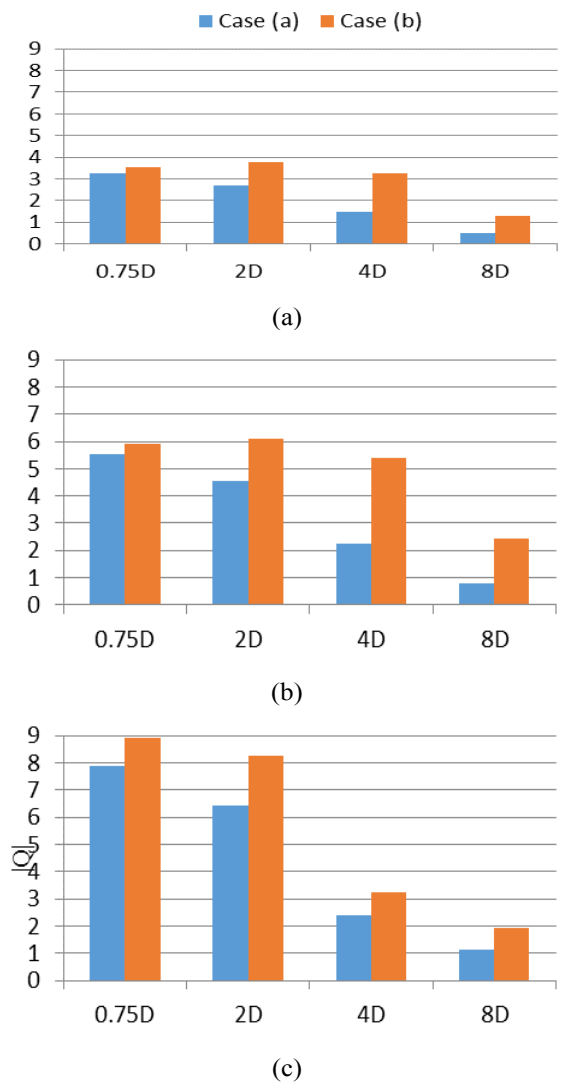

Figure-8. The dimensionless velocity defect flux ($|Q|$) for: case (a) Circular cantilever cylinder and case (b) Rectangular flat plate, where (a) AR=3; (b) AR=5, and (c) AR=7.

Based on Figure-9 and 10, it can be clearly observed that strong velocity defect is induced in the near wake (at x/D=0.75 and x/D=2) for both circular cantilever cylinder and rectangular flat plate. The velocity defect flux is up to -0.12 and -0.12~-0.15 for circular cantilever cylinder and rectangular flat plate respectively. However, the magnitude of the defect is almost the same at every distinct location. The increase of AR does not seem to have significant effect on the velocity defect flux at any location. At further downstream (x/D=4 and x/D=8), the vortical structure in the wake begins to loss its identity and its size is reduced. In this case, the velocity defects are mostly due to the shear stress generated at the floor. This statement is confirmed by the vorticity contours in Figure-6 and Figure-7. In this far downstream region, the vertical structures are presence near the floor. Thus, the dQ appears to be higher near the floor, which is approximately -0.08.

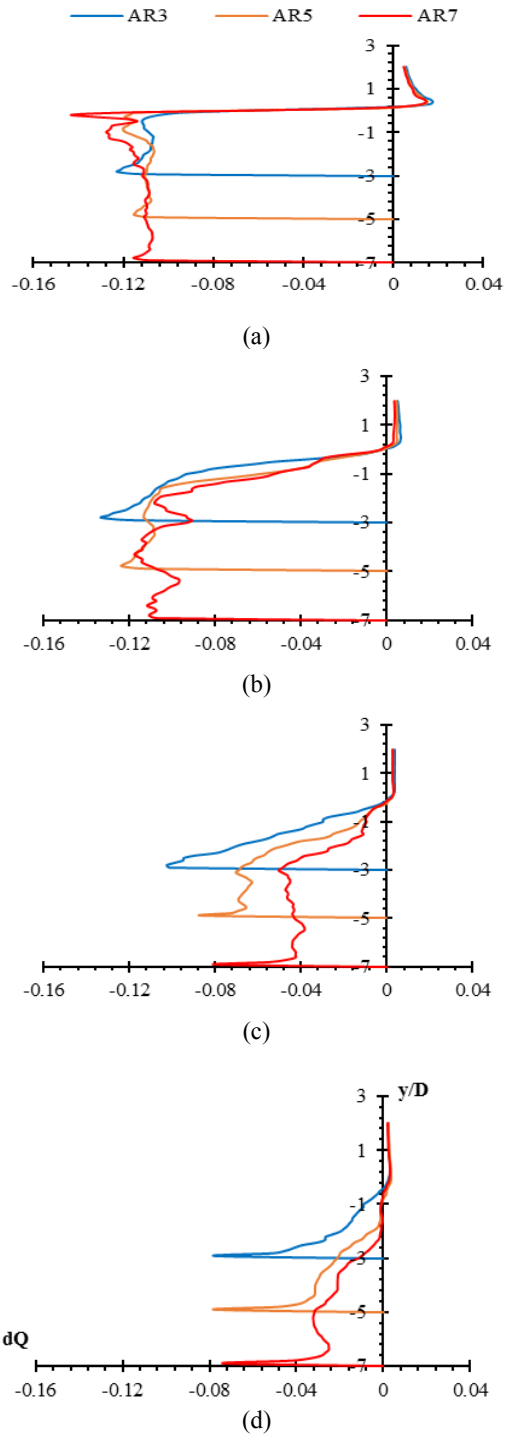

Figure-9. The dimensionless velocity defect flux of each tiny section (dQ) for circular cantilever at (a) x/D=0.75; (2) x/D=2, (3) x/D=4 and (4) x/D=8.

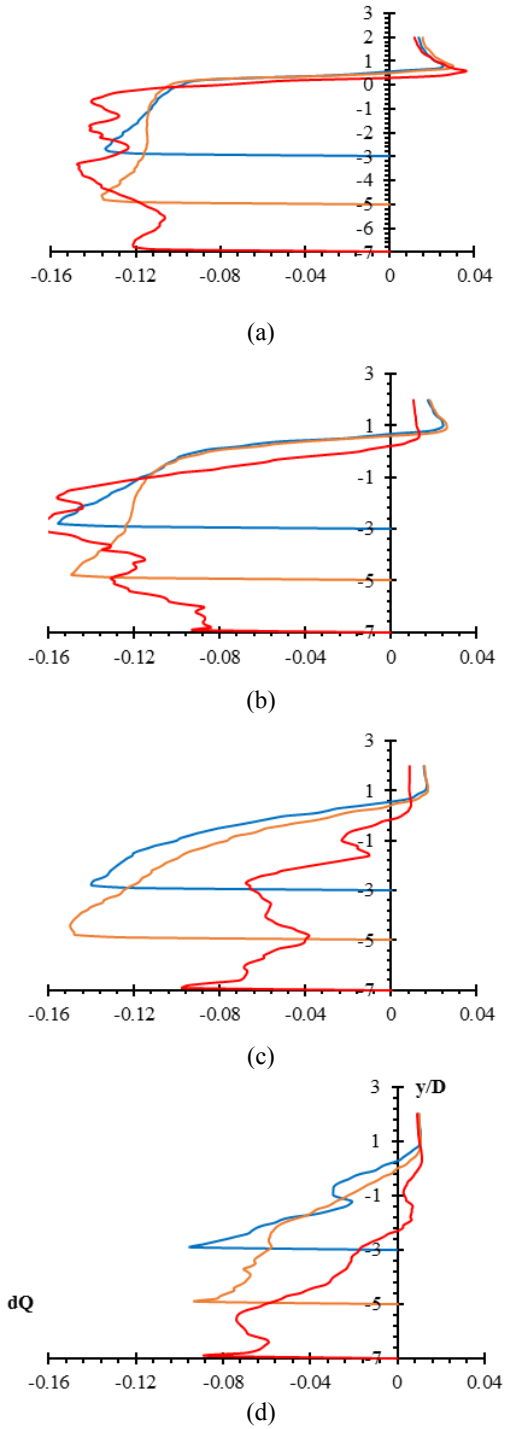

Figure-10. The dimensionless velocity defect flux of each tiny section (*dQ*) for rectangular flat plate at (a) *x/D*=0.75; (b) *x/D*=2, (c) *x/D*=4 and (d) *x/D*=8.

Influence of cross-sectional shape

Velocity defect is seen for both circular cantilever cylinder and rectangular flat plate from Figure-4 and they are particularly noticeable in the near-wake region. The magnitudes of the velocity defect for both circular cantilever cylinders and rectangular flat plate are summarized in Figure-8. The flow behavior in rectangular flat plate is, in general, similar to circular cantilever cylinder but with a greater magnitude overall. The velocity defect of the rectangular cantilever is stronger than circular cantilever, by at least 6.81% up to 206.41% ranging from AR=3 to AR=7 at different streamwise location. Apart from that, it is worth stating that the high magnitude velocity defect is extended up to *x/D*=4 instead of only *x/D*=2 for circular cantilever cylinder. The velocity is recovered slowly and not as apparent as the circular cantilever cylinder except for AR=3.

To understand why the magnitude is higher for rectangular flat plate, it is essential to take a closer look at the velocity defect. By adopting the idea of potential flow, which is characterized by an irrotational velocity field, $\nabla \times \vec{v} = 0$, the streamlines for an incompressible potential flow around a circular shape object will exhibit an ideal state, as illustrated in Figure-11. Based on the figure, no separation is present and hence, it is clear that there is no velocity defect in the near wake (on the plane of symmetry). Therefore, by comparing the idealized flow field with the obtained data, a direct relationship between the velocity defect and vortical motions can be deduced; where the velocity defect is a direct consequence of the presence of vortical motion in the flow field, which show good agreement with the statement raised in previous discussion.

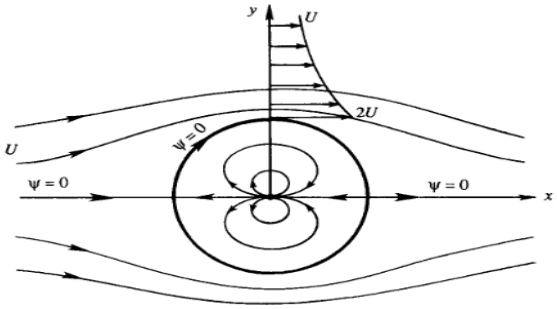

Figure-11. Streamlines for incompressible potential flow around a circular cylinder (Kundu and Cohen, 2010)

To form the vortical structures, the vortical structures must be constantly fed with energies. This type of energy transfer can be explained by the kinetic energy budget equation, equation (6):

$$\frac{D}{Dt}\left(\overline{\frac{1}{2}u_i^2}\right) = -\frac{\partial}{\partial x_j}\left(-\frac{\overline{pu_j}}{\rho_0} + \frac{1}{2}\overline{u_i^2 u_j} - 2\nu\overline{u_i e_{ij}}\right) - 2\nu\overline{e_{ij}e_{ij}} - \overline{u_i u_j}\frac{\partial U_i}{\partial x_j} - g\alpha\overline{\omega\Gamma} \quad (6)$$

where the vortical structures gain its energy from the mean flow through shear, which is represented by the

term $-\left(\overline{u_i u_j}\frac{\partial U_i}{\partial x_j}\right)$ in equation (6). During the formation of the vortical structures, the structures in the near wake has to extract energy from the mean flow resulting in the decrease of velocity in the mean flow. Thus, one could see a higher turbulent energy content in the wake due to the mentioned energy transfer.

Turbulent Kinetic Energy (TKE) contours are presented in Figure-12 and 13 to show the influence of cross-sectional shape on the TKE generation. The TKE should be at highest in the region with greater velocity defect and slowly attenuate further downstream as velocity defect become less significant if the kinetic energy budget equation holds true. If one compares the TKE contours (Figure-12 and 13) with the velocity profiles (Figure-4 and 5), it is no surprise to see the results of both figures and the speculation match perfectly: the TKE is greater at the region with greater velocity defect because the vortical structures in the near wake are draining more energy from the mean flow and that leads to the reduction of the flow's velocity and vice versa for the TKE at further downstream.

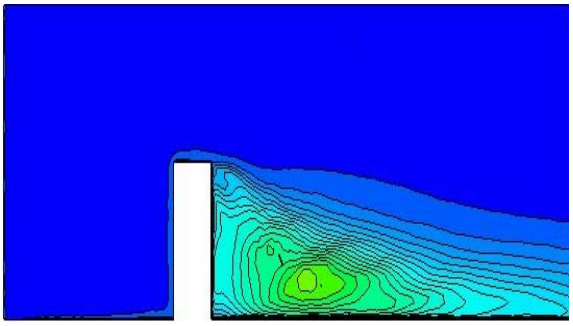

(a)

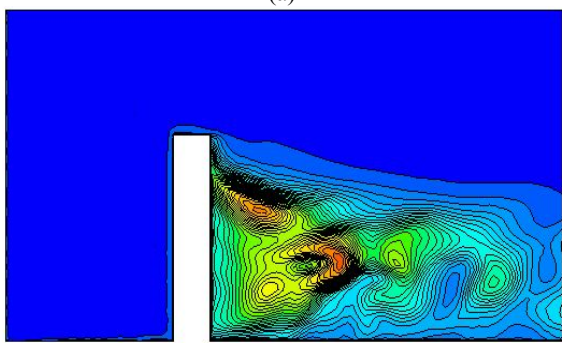

(b)

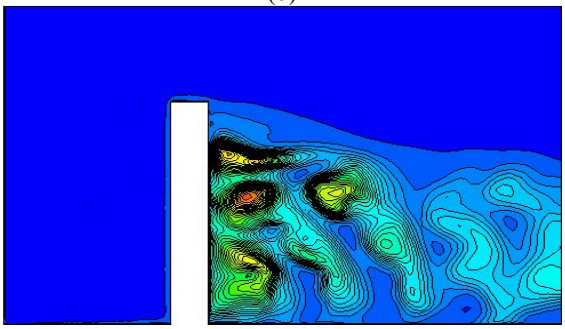

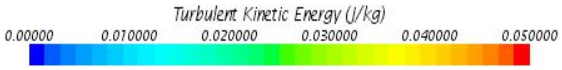

(c)

Figure-12. The instantaneous turbulent kinetic energy contour at the plane of symmetry at *t=2s* for circular cantilever, where (a) AR=3; (b) AR=5, and (c) AR=7.

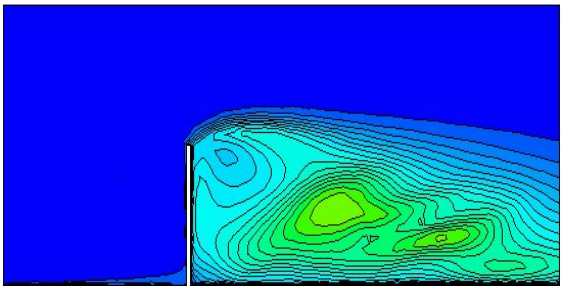

(a)

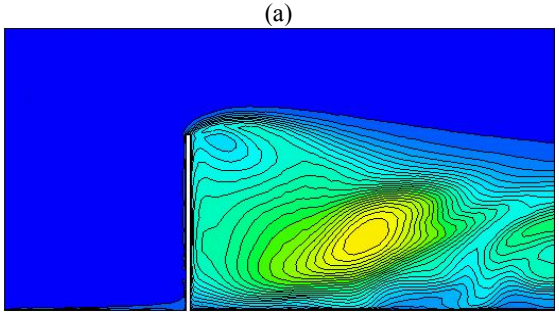

(b)

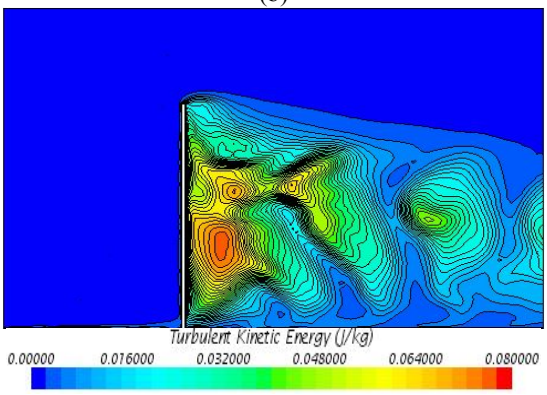

(c)

Figure-13. The instantaneous turbulent kinetic energy contour at the plane of symmetry at *t=2s* for rectangular flat plate, where (i) AR=3; (ii) AR=5, and (iii) AR=7.

The results show a direct relationship between the velocity defect and the vortical activities present in the flow field. The degree of velocity defect is a direct indicator of the level of vortical activities in the studied region and one could expect a higher TKE in a wake with large velocity defect compared to the case that has weaker velocity defect.

From the TKE contours (Figure-12 and 13), it is observed that the TKE content for rectangular flat plate is comparatively higher than that of circular cantilever cylinder, whereby the maximum TKE of rectangular flat

plate case is approximately 20%~50% higher than circular cantilever case. This may be due to the presence of the discontinuity point, *i.e.* the sharp edges of the rectangular flat plate. The velocity gradient at a discontinuity point is generally greater than other locations in the flow field and is notably greater than that of the surface of a blunt body. This phenomenon can be seen from the velocity profiles (Figure-4 and 5) and velocity field plots (Figure-14), where a greater velocity gradient is present at the tip of rectangular cantilever compared to circular cantilever. Enormous shear is produced as a result of the high velocity gradient. Through the shear production, colossal amount of energy is then transferred to the vortical structure. Contours of vorticity are shown in Figure-6 and 7. It is observed that the vorticity magnitude is independent to the cross-sectional shape. The magnitude of the vorticity of same AR for circular cantilever cylinder and rectangular flat plate is nearly similar. However, the vortical structures for the rectangular flat plate are larger than that of circular cantilever cylinder. It can be from the circulation theorem that the larger area of the vortical structure would yield a greater strength given the same vorticity. Therefore, it can be said that the strength for rectangular flat plate is higher than that of circular cantilever cylinder.

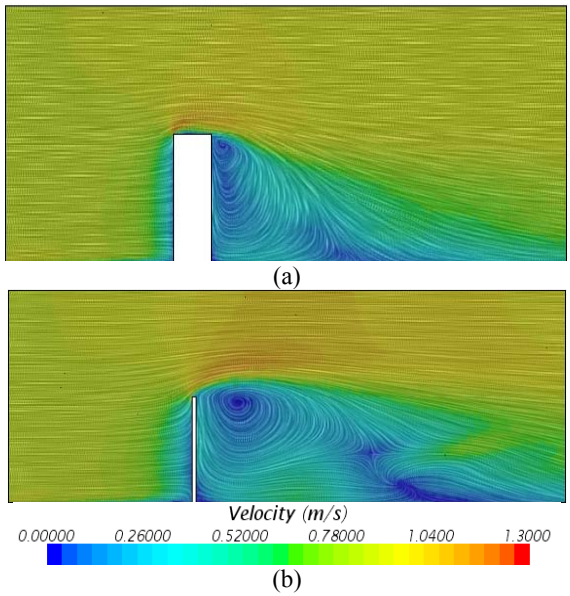

Figure-14. The instantaneous velocity field at the plane of symmetry when *t=2s* for: (a) Circular Cantilever Cylinder with AR=3 and (b) Rectangular Flat Plate with AR=3

CONCLUSIONS

This paper studies the effects of AR and geometry have on a finite cylinder at Re= $2x10^4$ using Star CCM+. It was numerically simulated by RANS. A circular cantilever cylinder and a rectangular flat plate with AR = 3, 5, 7 were tested. The following conclusions were obtained.

- Influences of AR: The tip effects are limited up to three diameters from the top of the circular cantilever cylinder and up to four diameters from the top of the rectangular flat plate. The effective area of the tip effects is independent to the AR. It could be influenced by the properties of the flow and fluid. Further investigations are needed to justify the hypothesis.
- Influences of cross-sectional shape: In general, rectangular cross-sectional shape generates stronger vortical structures compared to circular cross-sectional shape. Based on the TKE, the maximum TKE is approximately 20%~50% higher in rectangular flat plate when compared to circular cantilever cylinder at each respective *AR*. This can be caused by the presence of more discontinuity points on the rectangular geometry. The presence of discontinuity points, i.e. sharp edges on the rectangular flat plate can induce a greater velocity defect. In other words, it has the ability to preserve higher energy content in the flow field compared to circular cantilever cylinder. The high energy flow field generated at the discontinuity point also leads to greater effective area of the tip effects. From the study, the effective area of the tip effect for the rectangular cross-section case is $y/D \approx$ -3 to -4, which is approximately 1*D* to -2*D* larger than circular cross-section case ($y/D \approx$ -1 to -3).

Aside from the major findings listed above, the following can also be concluded:

- The magnitude of the velocity defect can be quantified by computing the velocity defect flux, *Q*. Greater *Q* indicates a greater velocity defect.
- Velocity defect can be a direct indicator of the presence of vortical motion in the wake and its magnitude represents the degree of vortical motion in the wake.

REFERENCES

[1] Afgan, I., Moulinec, C., Prosser, R. and Laurence, D. (2007). Large eddy simulation of turbulent flow for wall mounted cantilever cylinders of aspect ratio 6 and 10. International Journal of Heat and Fluid Flow, 28(4), 561-574.

[2] Afgan, I., Moulinec, C. and Laurence, D. (2006). Large eddy simulation of flow over a vertically mounted finite cylinder on a flat plate. In Conference on Modelling Fluid Flow (CMFF 2006). The 13th International Conference on Fluid Flow Technologies, Budapest, Hungary.

[3] Dol, S. S. and Nor, M. A. M. (2006). Flow visualization of the vortex shedding of a stationary circular cylinder by an improved smoke-wire technique. WSEAS transactions on fluid mechanics, 1(6), 745.

[4] Heseltine, J. L. (2003). Flow around a circular cylinder with a free end. (Master's Thesis, University of Saskatchewan, Saskaton, Saskatchewan, Canada) Retrieved from http://ecommons.usask.ca/handle/10388/etd-07252011-090143.

[5] Javadi, K. and Kinai, F. (2014). On the Turbulent Flow Structures over a Short Finite Cylinder: Numerical Investigation. Proceedings of the International Conference on Heat Transfer and Fluid Flow, no. 129 .

[6] Krajnović, S. (2011). Flow around a tall finite cylinder explored by large eddy simulation. Journal of Fluid Mechanics, 676, 294-317.

[7] Kundu, P. K. and I. M. Cohen. (2010). Fluid mechanics. 4th ed. Academic Press.

[8] Menter, F. R. (1994). Two-equation eddy-viscosity turbulence models for engineering applications. AIAA journal, 32(8), 1598-1605.

[9] Okamoto, T. and Yagita, M. (1973). The experimental investigation on the flow past a circular cylinder of finite length placed normal to the plane surface in a uniform stream. Bulletin of JSME, 16(95), 805-814.

[10] Palau-Salvador, G., Stoesser, T., Fröhlich, J., Kappler, M. and Rodi, W. (2010). Large eddy simulations and experiments of flow around finite-height cylinders.Flow, turbulence and combustion, 84(2), 239-275.

[11] Park, C. W. and Lee, S. J. (2000). Free end effects on the near wake flow structure behind a finite circular cylinder. Journal of Wind Engineering and Industrial Aerodynamics, 88(2), 231-246.

[12] Ringuette, M. J., Milano, M. and Gharib, M. (2007). Role of the tip vortex in the force generation of low-aspect-ratio normal flat plates. Journal of Fluid Mechanics, 581, 453-468.

[13] Roh, S. and Park, S. (2003). Vortical flow over the free end surface of a finite circular cylinder mounted on a flat plate. Experiments in fluids, 34(1), 63-67.

[14] Williamson, C. H. (1996). Vortex dynamics in the cylinder wake. Annual review of fluid mechanics, 28(1), 477-539.